Doppler Angle Estimation Using Correlation

Pai-Chi Li, *Member, IEEE*, Chong-Jing Cheng, and Che-Chou Shen

***Abstract*—Conventional Doppler techniques can only detect the axial component of blood flow. To obtain the transverse flow component, an approach based on the dependence of Doppler bandwidth on Doppler angle has been widely investigated. To compute the bandwidth, a full Doppler spectrum is often required. Therefore, this approach has not been applied to real-time, two-dimensional Doppler imaging because of the long data acquisition time. To overcome this problem, a correlation-based method is proposed. Specifically, variance of the Doppler spectrum is used to approximate the square of the Doppler bandwidth. Because variance is computed efficiently and routinely in correlation-based color Doppler imaging systems, implementation of this method is straightforward. In addition, the two-dimensional velocity vector can be calculated and mapped to different colors using the color mapping function of current systems. Simulations were performed, and experimental data were also collected using a string phantom with the Doppler angle varying from 23° to 82°. Results indicate that the correlation-based method may produce significant errors if only a limited number of flow samples are available. With averaging, however, the Doppler angles estimated by the correlation-based method can achieve good agreement with the true angles by using only four flow samples with proper variance averaging.**

I. Introduction

The Doppler effect resulting from ultrasound's interaction with moving red blood cells has been used extensively to determine blood flow velocity. A major problem of Doppler techniques is that only the axial flow component can be detected. The projection of the velocity vector onto the transverse direction does not produce Doppler shift. Therefore, transverse flows are undetectable through the Doppler shift only. To obtain two- or three-dimensional flow information, a number of techniques have been proposed [1]–[10].

One approach is the speckle tracking method [1]–[3]. This method relies on the assumption that speckle translation closely reflects target translation at small displacements. Hence, the two-dimensional velocity vector can be found by tracking the speckle patterns from consecutive B-mode images. However, because the speckle patterns are more decorrelated at larger translations, rapid image acquisition is necessary, and the performance of this method is limited. In addition, this method requires a large number of real-time computations.

Another approach for two-dimensional flow estimation is to use two beams crossing each other in the region of interest [4]. These beams originate from different positions of the transducer, producing different Doppler angles. The axial velocity components from the two measurements are then combined with geometric relationships to obtain the two-dimensional velocity vector. To achieve adequate accuracy, the angle between the beams needs to be sufficiently large. Therefore, a large transducer is required, making this method inappropriate for cardiac applications. Moreover, the need to produce simultaneous beams increases system complexity. Another multi-beam approach was also explored for three-dimensional flow estimation [5], [6]. This method utilizes three parallel and closely spaced beams. As scatterers move across beams, the three-dimensional velocity vector can be calculated by correlating signals from the three beams. Success of this technique is determined by the ability to produce beams with desired characteristics, such as beam width, beam spacing, focal distance, and depth of field [5], [6].

The transverse flow velocity component can also be found using the Doppler bandwidth [7]–[10]. Assuming negligible velocity variation within the sample volume and sufficient velocity resolution, it was shown that the Doppler bandwidth is inversely proportional to the transit time of a scatterer crossing the ultrasound beam in the focus of a transducer [11]. This is also known as the transit time spectrum broadening effect. Equivalently, Doppler spectrum broadening can also be attributed to the geometrical spectrum broadening effect caused by scatterers in the sample volume, which produce a range of Doppler angles. In both cases, the Doppler bandwidth may vary with the flow angle. Therefore, it is possible to calculate the transverse flow component given the Doppler bandwidth and ultrasound beam geometry. To estimate the Doppler bandwidth accurately, however, a complete Doppler spectrum is often required. In other words, this method is only suitable for spectral Doppler modes such as pulsed wave (PW) Doppler and continuous wave (CW) Doppler. Consequently, the Doppler angle can only be estimated in the region of interest. For real-time, two-dimensional Doppler angle estimation, efficient estimation of the Doppler bandwidth is necessary.

In this paper, a correlation-based method for Doppler angle estimation is proposed. Instead of calculating the Doppler bandwidth based on a complete spectrum, variance of the spectrum is used to approximate the square of the Doppler bandwidth. Because variance is calculated routinely in correlation-based color Doppler imaging systems, implementation of this approach is straightforward. In addition, calculation and display of the two-dimensional velocity vector can be implemented using a two-dimensional look-up table. Such a mapping function

Manuscript received April 13, 1999; accepted September 15, 1999.
The authors are with the Department of Electrical Engineering, National Taiwan University, Taipei, Taiwan, R.O.C. (e-mail: paichi@cc.ee.ntu.edu.tw).

already exists in current color Doppler imaging systems. Therefore, real-time flow imaging with automatic angle correction only requires minimum modifications to current commercial ultrasonic imaging systems.

The paper is organized as follows. Section II describes principles of the correlation-based method. Dependence of the Doppler bandwidth on the Doppler angle is also discussed. In Section III, simulation results, assuming a single scatterer, are presented. Doppler bandwidths derived from complete spectra are also compared with variance values obtained from the correlation processing. In Section IV, performance of this method is investigated with experimental data using a string phantom. The paper concludes in Section V with a discussion on system implementation issues and potential limitations.

II. Correlation-Based Doppler Angle Estimation

Analysis of the transit time spectrum broadening effect is based on the following assumptions. First, flow turbulence and velocity gradient are negligible. Hence, they do not contribute to spectral broadening. Second, frequency resolution of the spectral estimator is sufficient such that the spectrum broadening effect can be measured accurately. For example, if N-point discrete Fourier transformation is used to calculate the Doppler spectrum, the frequency resolution is roughly $1/N$ of the pulse repetition frequency (PRF). As a result, the transit time effect cannot be observed correctly if the Doppler bandwidth is smaller than PRF/N. The third assumption is that the transit time is governed by the ultrasound beam width instead of the range cell length. As illustrated in Fig. 1, this assumption is valid when the beam width w is considerably smaller than the range cell length l. In other words, the aspect ratio, defined as l/w, must be sufficiently large. Under these assumptions, the transit time t_{tr} through the ultrasound beam in the focus is

$$t_{\text{tr}} = \frac{w}{v \cdot \sin\theta} \tag{1}$$

where v is the single-valued flow velocity and θ is the Doppler angle. Because the Doppler bandwidth bw is inversely proportional to the transit time, we have

$$\text{bw} = k \cdot \frac{v \cdot \sin\theta}{w} \tag{2}$$

where k is a scaling factor related to the thresholds used to define bw and w. By combining bandwidth bw with the axial velocity component $v \cdot \cos\theta$, we obtain

$$\frac{\text{bw}}{\text{v} \cdot \cos\theta} = \frac{k}{w} \tan\theta. \tag{3}$$

Therefore, given a Doppler spectrum and ultrasound beam geometry, the Doppler angle θ can be found by

$$\theta = \tan^{-1}\left(\frac{w \cdot \text{bw}}{k \cdot v \cdot \cos\theta}\right). \tag{4}$$

Apparently, accuracy of Doppler angle estimation is determined by accuracy of the spectral estimator. In spectral Doppler modes (i.e., PW and CW), the fast Fourier transformation (FFT)-based spectral estimator typically is used to derive the Doppler spectrum. In this case, the axial velocity component $v \cdot \cos\theta$ and bandwidth bw can be readily obtained. However, the spectral Doppler modes only assess flow information within the Doppler gate or along a particular direction. Thus, the Doppler angle can only be estimated in a particular region of interest. For real-time two-dimensional Doppler angle estimation, alternative spectral estimation methods are required.

Another spectral estimation method commonly used in medical ultrasound is the correlation-based method for color Doppler imaging [12]. Instead of deriving complete Doppler spectra, this method only calculates specific spectral parameters, such as mean velocity and spectral variance. Nevertheless, the Doppler angle θ can still be found based on (4) using variance to approximate the square of the Doppler bandwidth. Note that the correlation-based method requires fewer samples for the estimation, thus making it suitable for real-time, two-dimensional velocity vector estimation. In addition, because the two parameters are routinely calculated, implementation of Doppler angle estimation is straightforward.

Let $P(\omega)$ represent a Doppler power spectrum, the spectral variance σ^2 is defined as

$$\sigma^2 \equiv \frac{\int_{-\infty}^{\infty} (\omega - \bar{\omega})^2 P(\omega)\, d\omega}{\int_{-\infty}^{\infty} P(\omega) d\omega} \tag{5}$$

where $\bar{\omega}$ is the mean Doppler angular frequency [12]. Assuming $P(\omega)$ is a Gaussian function, i.e.,

$$P(\omega) = e^{-\pi\left(\frac{\omega-\bar{\omega}}{\sigma_\omega}\right)^2} \tag{6}$$

where σ_ω corresponds to the -6.82-dB Doppler bandwidth, it is straightforward to obtain

$$\sigma^2 = \frac{\sigma_\omega^2}{2\pi}. \tag{7}$$

Therefore, variance is linearly proportional to the square of the -6.82-dB bandwidth of a Gaussian power spectrum. Of course, real physiological flows are unlikely to be exactly Gaussian distributed. Nevertheless, it is still reasonable to use spectral variance as an effective measure of the Doppler bandwidth. This hypothesis will be tested using both simulations and experimental data.

The following derivation of correlation-based variance calculation follows the descriptions in [12]. Assuming $S(t)$ is the received Doppler signal, the auto-correlation function $R(t)$ of $S(t)$ is defined as

$$R(t) \equiv \int_{-\infty}^{\infty} S^*(t+\tau) S(\tau) d\tau \tag{8}$$

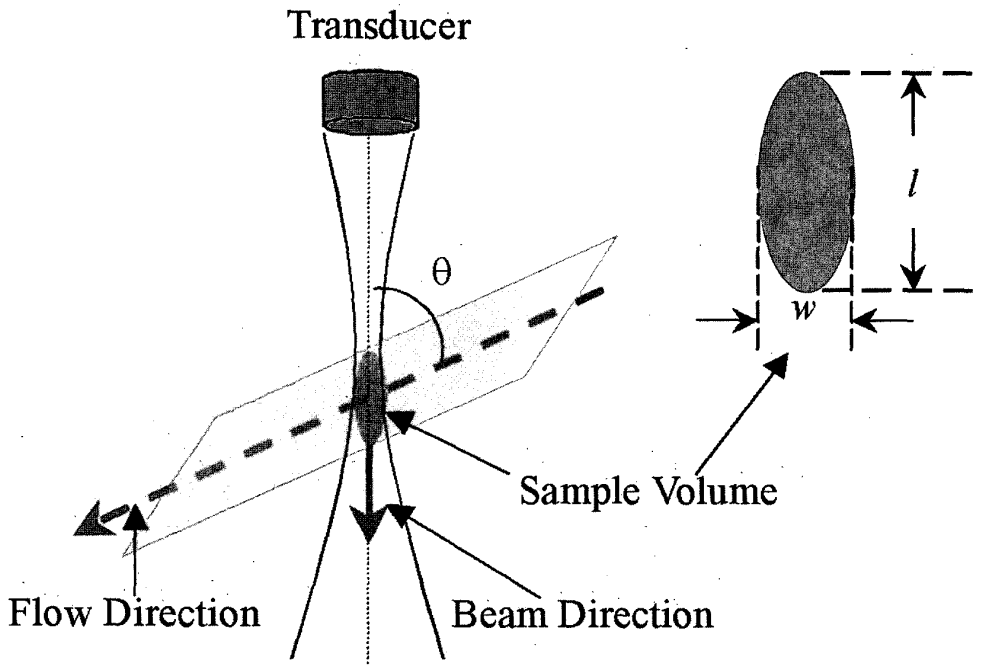

Fig. 1. Schematic representation of Doppler angle and sample volume geometry.

where $*$ represents the complex conjugate. Based on the Wiener-Khinchin theorem, the mean Doppler angular frequency $\bar{\omega}$ is

$$\bar{\omega} = \frac{\int_{-\infty}^{\infty} \omega P(\omega) d\omega}{\int_{-\infty}^{\infty} P(\omega) d\omega} = -j\frac{R'(0)}{R(0)} \tag{9}$$

where $R'(0)$ is the first-order differential of $R(t)$ evaluated at $t = 0$. The variance, on the other hand, can be approximated by

$$\sigma^2 \approx \frac{2}{T^2}\left[1 - \frac{|R(T)|}{R(0)}\right] \tag{10}$$

where T denotes the emission interval of ultrasound pulses (i.e., PRF $= 1/T$).

In pulsed Doppler modes (i.e., PW and color Doppler), (8) needs to be modified. First, the continuous signal $S(t)$ is sampled at PRF. Second, $R(t)$ can be calculated based on a finite number of samples only. Assuming the number of available samples is N, $R(0)$ and $R(T)$ are typically approximated by an unbiased Blackman-Tukey estimator with the following forms:

$$\hat{R}(0) = \frac{1}{N}\sum_{i=1}^{N} S^*(i \cdot T) S(i \cdot T), \tag{11}$$

$$\hat{R}(T) = \frac{1}{N-1}\sum_{i=1}^{N-1} S^*\left((i+1) \cdot T\right) S(i \cdot T). \tag{12}$$

Unfortunately, this estimator may lead to a negative variance value because the unbiased sequence does not guarantee a positive semidefinite sequence [13]. To ensure positive variance values, an alternative estimator for $R(0)$ is used:

$$\hat{R}(0) = \frac{1}{2(N-1)}\sum_{i=1}^{N-1}\left[|S(i \cdot T)|^2 + |S\left((i+1) \cdot T\right)|^2\right]. \tag{13}$$

By combining (10) and (13), it is straightforward to verify that σ^2 is always positive.

Because the correlation-based method typically uses a smaller number of samples, estimation errors may be significant and are likely to affect the accuracy of bandwidth estimation. In addition, the frequency resolution is also degraded and may be insufficient to measure the spectrum broadening effect. To reduce such errors, variance estimates may be averaged spatially, temporally, or both. Assuming that the flow angle does not vary significantly in the image plane, neighboring variance estimates can be averaged to compute the Doppler bandwidth. Alternatively, temporal averaging can be performed, assuming that the flow characteristics remain relatively constant temporally. Efficacy of averaging will be verified experimentally.

III. Single Scatterer Simulations

The previous analysis assumed that the Doppler bandwidth is related directly to transit time. However, if the observation time [i.e., $(N-1)^*T$] is smaller than the transit time, dependence of the Doppler bandwidth on the Doppler angle no longer exists. In other words, if the distance that sound scatterers travel during the observation time is smaller than the path length along the flow direction (i.e., $w/\sin\theta$), Doppler bandwidth will be linearly

proportional to the inverse of the observation time, instead of the transit time. Therefore, the following condition must be satisfied to apply (4):

$$v \cdot (N-1) \cdot T \geq \frac{w}{\sin\theta}. \tag{14}$$

Equivalently,

$$\sin\theta \geq \frac{w}{v \cdot (N-1) \cdot T}. \tag{15}$$

Another critical issue is the aspect ratio. Ideally, l needs to approach infinity so that (1) is valid at all Doppler angles. However, it is practically impossible to have an infinite range cell length. In pulsed Doppler modes, l is finite because it is the combination of the length of the transmitted burst and the Doppler gate. In CW Doppler, l is also finite determined by attenuation, the intersection of transmit and receive beams, and the overlap of the ultrasound beam and the blood vessel. Thus, applicability of (1) is limited further because $w/\sin\theta$ may be larger than l at small Doppler angles. As a rule of thumb, a critical angle θ_c can be defined for large aspect ratios:

$$\theta_c \equiv \sin^{-1}\left(\frac{w}{l}\right) = \sin^{-1}\left(\frac{1}{\text{aspect ratio}}\right). \tag{16}$$

The Doppler angle must be greater than θ_c to be estimated based on (4). Note that practically the critical angle is larger than $\sin^{-1}(w/l)$ because the shape of the sample volume is not rectangular. Moreover, for sample volumes with an aspect ratio close to 1, the path length quickly becomes smaller than $w/\sin\theta$ as the Doppler angle decreases from 90°. Therefore, (16) becomes inapplicable [14], [15].

Dependence of the Doppler bandwidth on the Doppler angle, aspect ratio, and flow velocity is studied using simulations. The simulation method is similar to the one described in [16] and [17]. The simulation model assumes point scatterers randomly positioned in three-dimensional space. Geometry and diffraction effects of the transducer are also included. In all simulations, a single scatterer is assumed. In addition, the transducer has a center frequency of 5 MHz and an aperture size of 1 cm. The sample volume is located at the focal point, which is 2 cm away from the transducer. The −6-dB beam width is 0.54 mm, and the range cell length l is set depending on aspect ratio requirements. The sound propagation speed is 1540 m/s.

Effects of the aspect ratio on the −10-dB Doppler bandwidth are shown in Fig. 2. Doppler spectra are derived using 64-point FFT with a Hamming window, and the scatterer velocity is 60 cm/s. Three aspect ratios are investigated. Doppler bandwidths as a function of $\sin\theta$ with an aspect ratio of 1 are shown as the dashed line. Results of aspect ratios of 2 and 5 are shown as the dot-dashed line and the solid line, respectively. Finally, the dotted line denotes the ideal linear relationship between the bandwidth and $\sin\theta$.

For a ratio of 1, the sample volume becomes circular. Thus, Doppler bandwidth is relatively constant because the transit time does not change as a function of the Doppler angle. For a ratio of 5, the relationship between bandwidth and $\sin\theta$ is approximately linear at larger Doppler angles. At smaller angles, however, the linear relationship is not consistent because (2) becomes invalid. Because of the elliptical shape of the sample volume, the linear region starts from an angle larger than the critical angle defined by (16) [i.e., $\sin^{-1}(1/5)$]. For a ratio of 2, dependence of the Doppler bandwidth on $\sin\theta$ is significantly different from the ideal case denoted by the dotted line. This is due to the fact that, with a small aspect ratio and an elliptical sample volume, the path length along the flow direction quickly deviates from $w/\sin\theta$ as the Doppler angle decreases from 90°. Thus, Fig. 2 indicates that an aspect ratio < 5 may be inadequate for Doppler angle estimation under most imaging situations.

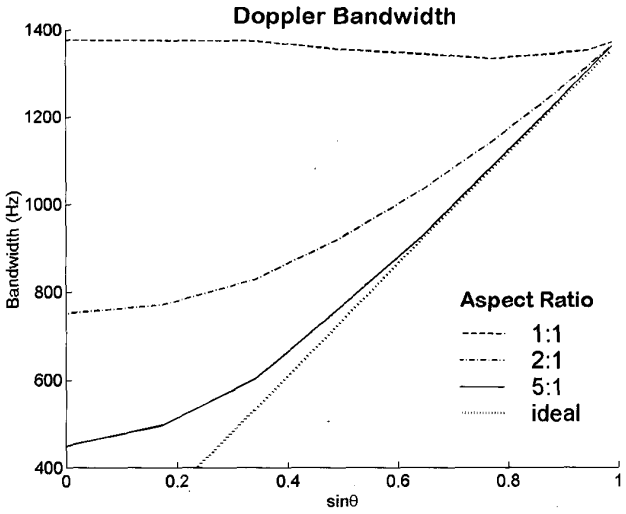

Fig. 2. Effects of aspect ratio on Doppler bandwidth.

Dependence of the Doppler bandwidth on the scatterer velocity is shown in Fig. 3. In all cases, the aspect ratio is 5. The three curves correspond to scatterer velocities at 60, 40, and 20 cm/s (from top to bottom). It is shown that, as the velocity increases, the critical angle decreases, and the slope in the linear region increases.

The correlation-based method is also compared with the FFT-based method. In Fig. 4, the dashed line shows −6.82-dB bandwidths obtained from the FFT method, and the solid line shows bandwidths estimated using the variance based on (7) and (10) (i.e., bw = $\sqrt{2\pi}\sigma$). The number of samples is 64 in both cases for comparison purposes. Note that the typical number of samples used in correlation-based imaging systems is between 4 and 12. Generally, the two methods have good agreement even though the Doppler spectrum is non-Gaussian. Therefore, the validity of using variance to measure the Doppler bandwidth is verified, assuming the same number of samples is used. Efficacy of the correlation-based method with a smaller number of samples will be discussed in the subsequent sections.

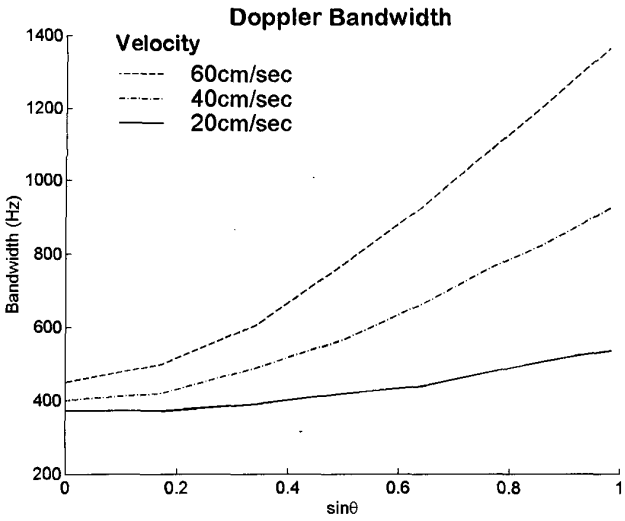

Fig. 3. Effects of flow velocity on Doppler bandwidth.

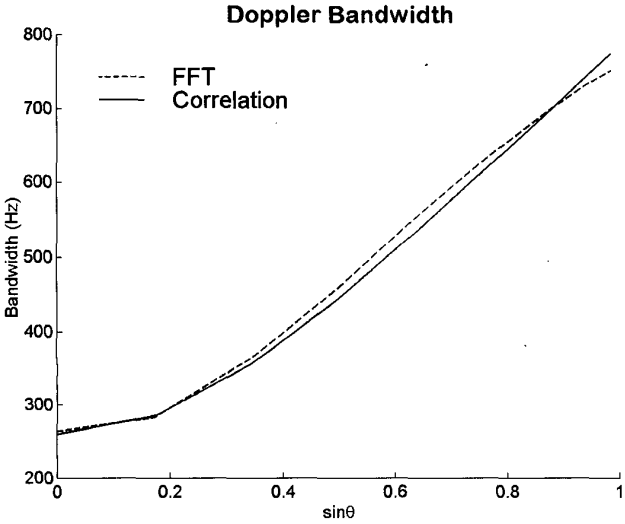

Fig. 4. Comparison of the FFT-based method to the correlation-based method.

IV. Experimental Results

The correlation-based method was applied to string phantom data as an empirical proof of concept. A block diagram of the experiment system is shown in Fig. 5. The data acquisition system consisted of a pulser/receiver (5072PR, Panametrics, Massachusetts) and a VXI mainframe (Hewlett-Packard, California) with a 12-bit, 40-Msamples/s arbitrary function generator and a 12-bit, 20-Msamples/s A/D converter. The equipment was controlled by a personal computer via VEE software (Hewlett-Packard). The arbitrary function generator was used to trigger the pulser externally with a pulse emission interval of 180 μs. After the returning echoes were amplified, the radio frequency (RF) signals were then sampled by the A/D converter and stored for off-line signal processing.

The transducer (V308-SU, Panametrics) had a center frequency of 5 MHz and a fixed focus at 70 mm. Diameter of the transducer was 19 mm, making the two-way, −6-dB beamwidth about 1 mm at the focal point.

The principles derived assume that the flow velocity throughout the sample volume is single valued. A string phantom was designed to meet this requirement. Flow was simulated by moving the string, which was made of a strap with a diameter of 5 mm. The strap was knotted into a loop and driven by pulleys 2 and 3. Note that a thick strap, instead of a thin thread, was used to mimic uniform motion of multiple scatterers. As shown in Fig. 5, pulley 1 was driven by a DC motor, and a string loop connecting pulleys 1 and 2 acted as a drive belt. Another string loop was connected between pulleys 2 and 3, and the upper portion of the string intersected with the ultrasound beam at the focal point of the transducer. The three pulleys were mounted on a plastic frame, and the Doppler angle was adjusted by changing positions of pulleys 2 and 3. The Doppler angles used in this paper were 23°, 38°, 44°, 62°, 71°, and 81°. The average string speed was around 35 cm/s. It was calculated by dividing the string length by the elapsed time for the string to travel a complete circle.

The receiver gate length was 7.5 mm, thus producing an aspect ratio of 7.5. With 64-point FFT for spectral analysis, the aspect ratio, PRF, and the string speed ensured that (4) was applicable for all Doppler angles used in the experiments.

During data collection, the instantaneous string velocity deviated from the average velocity because the speed of the DC motor was not constant. The solid line in Fig. 6 shows the measured instantaneous string velocity (projected onto the beam direction) as a function of time. The dashed line is the average velocity at about 25 cm/s. Such velocity variation increases the Doppler bandwidth and must be removed for accurate Doppler angle estimation.

Instantaneous string velocity can be calculated by measuring the differential phase between two consecutive signals. Let θ_i denote the phase difference between the ith and the $i-1$th signals, i.e.,

$$\theta_i = \tan^{-1}\left\{\frac{\mathrm{Im}\left[S^*(i\cdot T)\cdot S\left((i-1)\cdot T\right)\right]}{\mathrm{Re}\left[S^*(i\cdot T)\cdot S\left((i-1)\cdot T\right)\right]}\right\}. \tag{17}$$

The instantaneous string velocity v_i can be found by

$$v_i = \theta_i \cdot \frac{\lambda}{4\pi T} \tag{18}$$

where λ is the wavelength of the carrier. Note that (17) is only defined for $i = 2, \ldots, N$. The starting phase θ_1 is set to zero.

The average velocity $\bar{v}$ is related to the linear component of the unwrapped phase across N signals. In other words,

$$\bar{v} = \frac{1}{N-1}\sum_{k=1}^{N}\theta_k\left(\frac{\lambda}{2\pi T}\right). \tag{19}$$

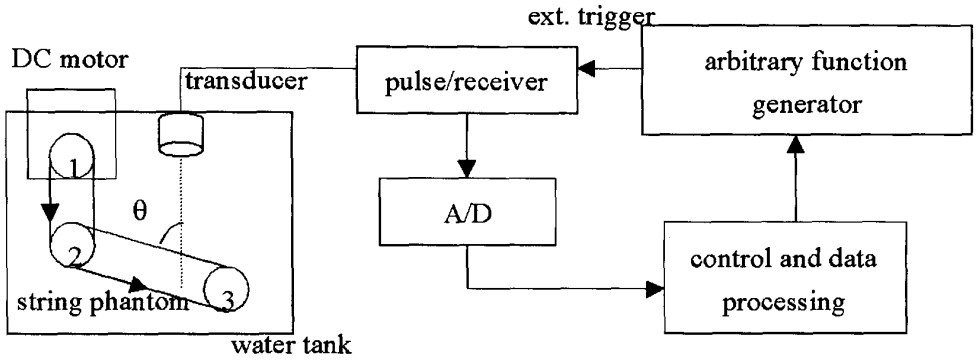

Fig. 5. Block diagram of the experimental set-up.

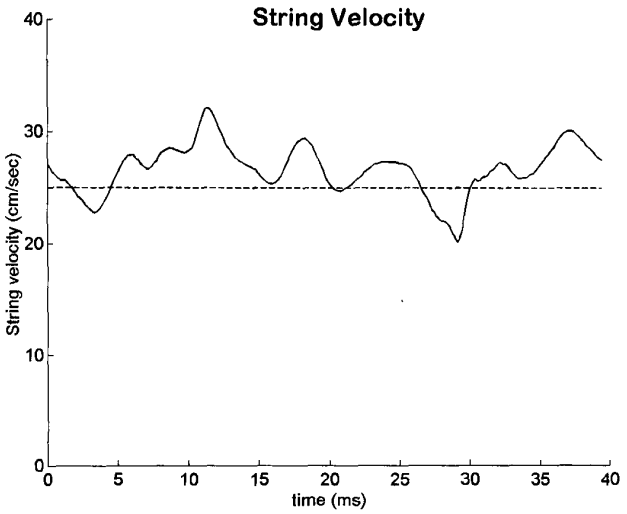

Fig. 6. Measured instantaneous string velocity.

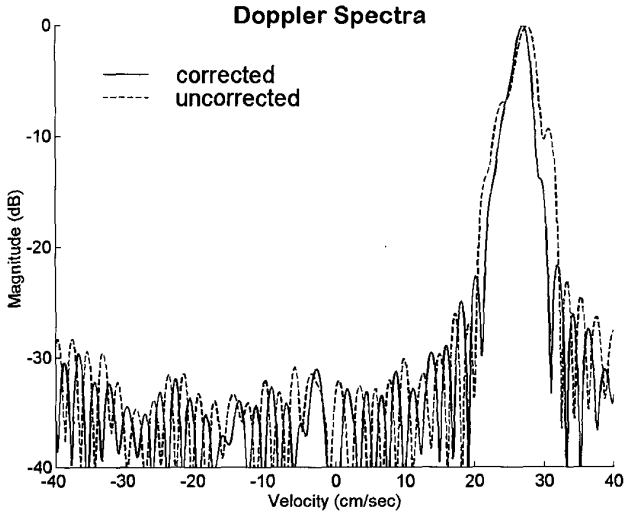

Fig. 7. Doppler spectra with (solid) and without (dashed) velocity variation correction.

By removing the linear component, the phase error $\Delta\theta_i$ can be defined as

$$\Delta\theta_i = \sum_{k=1}^{i} \theta_k - \frac{i-1}{N-1}\left(\sum_{k=1}^{N} \theta_k\right), \tag{20}$$

and the velocity variation Δv_i is

$$\Delta v_i = \Delta\theta_i \cdot \frac{\lambda}{2\pi T}. \tag{21}$$

String velocity variation can be corrected by removing $\Delta\theta_i$. In other words, the Doppler bandwidth is calculated based on a new signal defined as

$$\tilde{S}(i \cdot T) \equiv S(i \cdot T) \cdot e^{-j\Delta\theta_i} \tag{22}$$

where $\tilde{S}(i \cdot T)$ is simply a phase-rotated version of $S(i \cdot T)$. Note that the phase correction scheme described here is similar to the scheme developed for correcting sound velocity inhomogeneities [18], [19].

Fig. 7 shows spectra with (solid) and without (dashed) the removal of velocity variation. Clearly, velocity variation increases the Doppler bandwidth and may produce significant errors in Doppler angle estimation. The results shown in the rest of this section are all with string velocity variation correction.

Fig. 8 compares string phantom measurements with true Doppler angles. The solid line represents the tangent of the true Doppler angle at six string positions, and the solid line with circles denotes the tangent of the measured angle. A 64-point FFT with a Hamming window was used to derive the −6.82-dB bandwidths, and the k value described in (4) was empirically set to 11. The good agreement indicates that velocity variation is removed successfully. Furthermore, efficacy of the Doppler angle estimation scheme is verified. Fig. 9 shows −10-dB bandwidths from the same data with k set to 13.5. Although the estimation error slightly increases at larger Doppler angles, good overall conformance is still achieved. Note that the experiments were performed in the focal point, the phase error may also depend on the phase field distribution if out of focus [11], [20].

Results of the correlation-based method are shown in Fig. 10. Four flow samples (i.e., $N = 4$) with nine-point

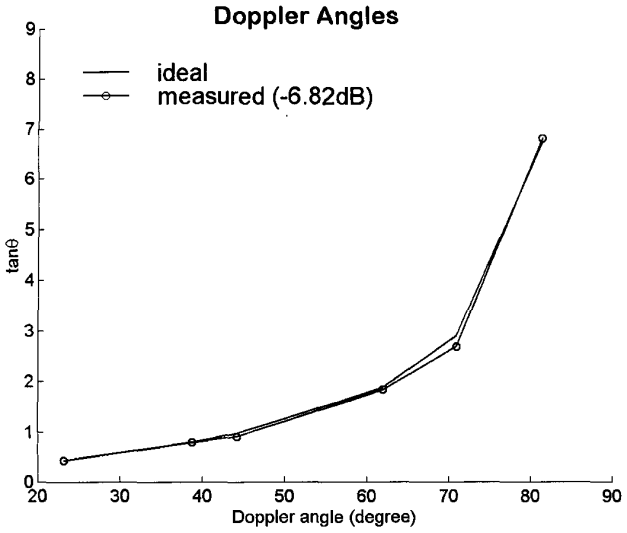

Fig. 8. Measured Doppler angles (solid with circles) vs. true Doppler angles (solid): −6.82-dB bandwidth.

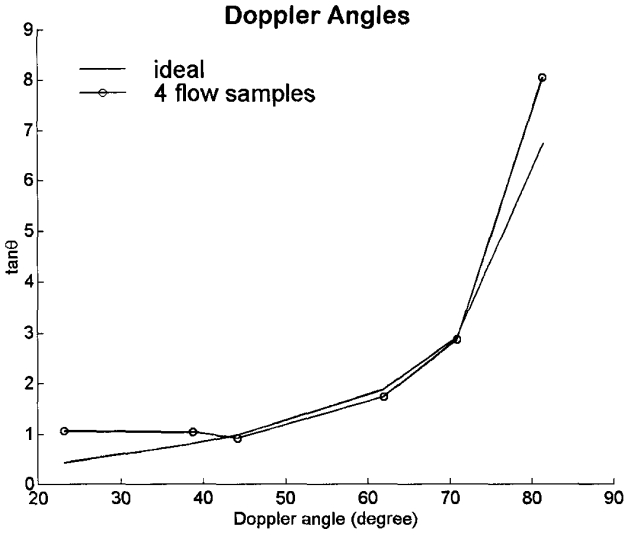

Fig. 10. Measured Doppler angles (solid with circles) vs. true Doppler angles (solid): correlation.

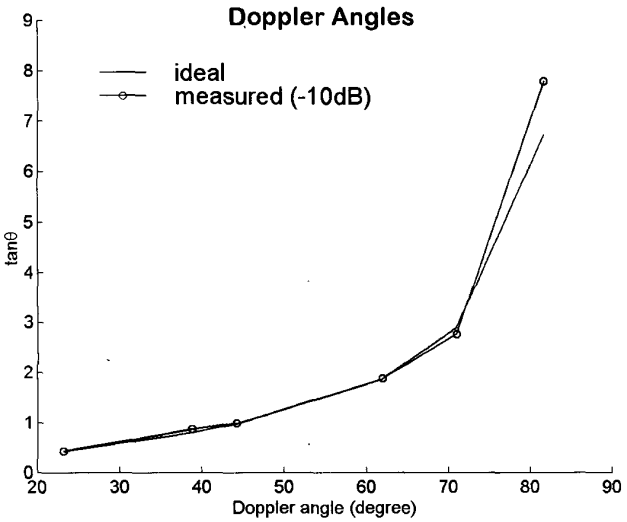

Fig. 9. Measured Doppler angles (solid with circles) vs. true Doppler angles (solid): −10-dB bandwidth.

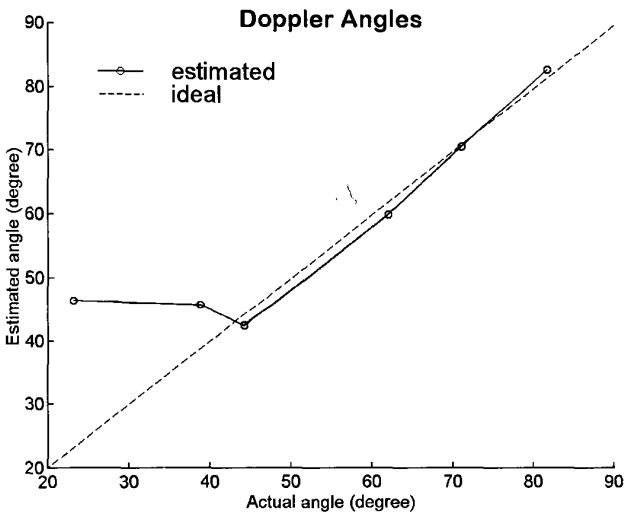

Fig. 11. Measured Doppler angles (solid with circles) vs. true Doppler angles (dashed): correlation.

averaging were used in all cases. According to (7), variance is linearly proportional to the square of the −6.82-dB bandwidth. Therefore, k was set to 11 such that it is consistent with the −6.82-dB results shown in Fig. 8. Note that averaging was performed on variance estimates from consecutive firings. In other words, 36 consecutive samples were used to derive nine variance estimates at each angle. Strictly speaking, this is different from both temporal averaging and spatial averaging in real imaging situations. Nevertheless, efficacy of estimation error reduction can still be tested using the current averaging scheme. Results with averaging are shown in Fig. 10 as the solid line with circles. Compared with the actual values shown as the solid line, conformance is good except at smaller Doppler angles. The nonconformance at smaller angles may be due to the fact that the effective number of samples is reduced from 64 for the FFT-based method to 36 for the correlation-based method. Therefore, the observation time becomes smaller than the transit time at smaller Doppler angles.

Without averaging, the estimated Doppler angles using only four samples are significantly different from the true angles. The reason for the nonconformance is twofold. First, estimation errors increase with fewer samples. Second, the observation time is smaller than the transit time at all angles. Therefore, the bandwidth is determined by the observation time instead of the transit time. Results without averaging are not shown because of significant errors. Note that averaging may not be required if the num-

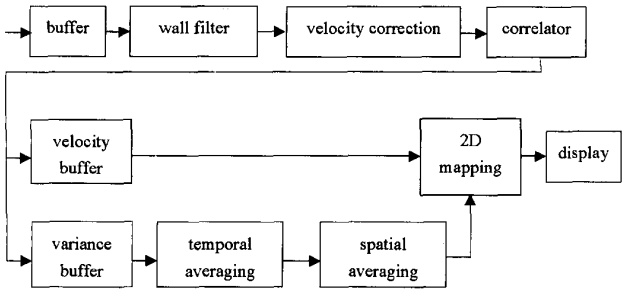

Fig. 12. Schematic diagram of a possible system architecture.

ber of samples is sufficiently large. As long as the observation time is larger than the transit time, the correlation-based results should have good agreement with the FFT-based results as indicated by Fig. 4. Fig. 11 illustrates the same results as in Fig. 10 with a different format. In this case, the estimated angles (denoted by the solid line with circles) are compared with the actual angles (denoted by the dashed line). Again, good conformance is achieved except for smaller angles.

V. Discussion and Concluding Remarks

In this paper, issues regarding Doppler angle estimation using the transit time spectrum broadening effect are discussed. Performance of the correlation-based method is also evaluated. The results suggest a possible system implementation scheme as shown in Fig. 12. Input data of the Doppler angle estimation system are complex baseband image data after receive beam formation. The data are stored in a buffer prior to the application of a wall filter to remove stationary and slow-moving signals. The flow velocity variation is then estimated and removed by rotating the phase of the baseband data. Note that, although this block is used to remove the velocity variation caused by motor inconsistency in this study, the approach proposed in this paper can be applied to any temporal velocity variation, such as the variation in a heart cycle. The phase-rotated data are sent to the correlator for mean velocity and variance estimation. To reduce estimation errors and to increase the effective observation time, the variance data are then temporally and/or spatially averaged before being combined with the velocity estimates. With the two-dimensional look-up table, the Doppler angle is calculated, and two-dimensional velocity vector information is encoded in color. Note that calculations for Doppler angle estimation, such as those described by (4), can be easily integrated into the look-up table. Therefore, the proposed architecture is efficient and only requires minimum modifications to current correlation-based Doppler imaging systems.

The transit time spectral broadening effect can be measured only if the observation time is longer than the transit time. It has been shown that the observation time can be increased by averaging the variance estimates obtained from consecutive firings. In this case, M-point averaging approximately increases the observation time by M times. The spatial and temporal averaging schemes depicted in Fig. 12, however, are different from the averaging scheme used in Fig. 10. For temporal averaging, the time interval between two consecutive variance estimates becomes the time required to acquire an image frame. For spatial averaging, on the other hand, the variance estimates are from different sample volumes. Although averaging can still be used to reduce estimation errors in both cases, efficacy of increasing the observation time by averaging may be significantly affected. Details of potential performance degradation and possible solutions are currently being explored.

A high aspect ratio is required to produce a small critical angle. On the other hand, a constant velocity within the sample volume is also required. Although these two requirements appear to contradict each other, both requirements can be satisfied by employing a summing scheme and correcting for the axial velocity variations. In this case, a short pulse is transmitted, producing a small sample volume. Thus, velocity variations within the sample volume can be minimized, and flow velocity within adjacent range cells can be independently estimated. After the velocity differences are calculated and removed, signals from adjacent range cells can be summed together to produce a longer sample volume. Hence, it effectively increases the aspect ratio without violating the constant flow assumption if the beam width is fixed. Assuming the flow direction does not change significantly in the neighboring region, adverse impact of the summing scheme is minimal.

To reduce system complexity, it is desired to have a fixed gate length regardless of the location of the sample volume. On the other hand, a fixed aspect ratio is also helpful for the interpretation of the final image. Consequently, a uniform beam width is required if a fixed gate length and a fixed aspect ratio are both necessary. Because current digital array imaging systems dynamically focus on receive, the uniform beam width requirement necessitates a large depth of field of the transmit beam. Hence, dynamic transmit focusing schemes, such as nondiffracting beams [21] and retrospective transmit focusing [22], are of particular interest for the real-time, two-dimensional Doppler angle estimation described in this paper. In addition, such schemes may reduce effects of the phase field distribution on Doppler bandwidth [11], [20]. If uniform beamwidth cannot be achieved, the summing scheme is advantageous because it offers a flexible control of the aspect ratio throughout the image.

Finally, the transverse flow estimation has been restricted to single-valued flows within the sample volume. Success of this method on turbulent flows or flows with non-negligible velocity gradient has not been reported in the literature. To address this issue, the velocity variation correction scheme described in this paper is currently being explored on time-varying and turbulent flows. In addition, effects of the summing scheme on flows with spatial velocity variation are also being investigated.

ACKNOWLEDGMENTS

The authors thank Dr. C.-K. Sun for laboratory assistance and the reviewers for the insightful comments.

REFERENCES

[1] G. E. Trahey, J. W. Allison, and O. T. von Ramm, "Angle independent ultrasonic detection of blood flow," *IEEE Trans. Biomed. Eng.*, vol. 34, no. 12, pp. 965–967, 1987.

[2] L. N. Bohs, B. H. Friemel, and G. E. Trahey, "Experimental velocity profiles and volumetric flow via two-dimensional speckle tracking," *Ultrason. Med. Biol.*, vol. 21, no. 7, pp. 885–898, 1995.

[3] L. N. Bohs, B. J. Geiman, M. E. Anderson, S. M. Breit, and G. E. Trahey, "Ensemble tracking for 2D vector velocity measurement: experimental and initial clinical results," *IEEE Trans. Ultrason., Ferroelect., Freq. Contr.*, vol. 45, no. 4, pp. 912–924, 1998.

[4] P. J. Phillips, S. W. Straka, and O. T. von Ramm, "Real-time two-dimensional vector velocity mapping ultrasound systems using subaperture pulse chasing," *Ultrason. Imag.*, vol. 18, no. 1, p. 60, 1996.

[5] I. A. Hein, "Triple beam lens transducers for three-dimensional ultrasonic fluid flow estimation," *IEEE Trans. Ultrason., Ferroelect., Freq. Contr.*, vol. 42, no. 5, pp. 854–869, 1995.

[6] ——, "3-D flow velocity vector estimation with a triple-beam lens transducer-experimental results," *IEEE Trans. Ultrason., Ferroelect., Freq. Contr.*, vol. 44, no. 1, pp. 85–95, 1997.

[7] V. L. Newhouse, E. S. Furgason, G. F. Johnson, and D. A. Wolf, "The dependence of ultrasound bandwidth on beam geometry," *IEEE Trans. Sonics Ultrason.*, vol. 27, no. 2, pp. 50–59, 1980.

[8] V. L. Newhouse, D. Censor, T. Vontz, J. A. Cisneros, and B. B. Goldberg, "Ultrasound Doppler probing of flows transverse with respect to beam axis," *IEEE Trans. Biomed. Eng.*, vol. 34, no. 10, pp. 779–789, 1987.

[9] P. Tortoli, G. Guidi, F. Guidi, and C. Atzeni, "A review of experimental transverse Doppler studies," *IEEE Trans. Ultrason., Ferroelect., Freq. Contr.*, vol. 41, no. 1, pp. 84–89, 1994.

[10] B.-R. Lee, H. K. Chiang, C.-D. Kuo, W.-L. Lin, and S.-K. Lee, "Doppler angle and flow velocity estimations using the classic and transverse Doppler effects," *IEEE Trans. Ultrason., Ferroelect., Freq. Contr.*, vol. 46, no. 1, pp. 252–256, 1999.

[11] O. W. Ata and P. J. Fish, "Effect of deviation from plane wave conditions on the Doppler spectrum from an ultrasonic blood flow detector," *Ultrasonics*, vol. 29, no. 5, pp. 395–403, 1991.

[12] C. Kasai, K. Namekawa, A. Koyano, and R. Omoto, "Real-time two-dimensional blood flow imaging using an autocorrelation technique," *IEEE Trans. Sonics Ultrason.*, vol. 32, no. 3, pp. 458–464, 1985.

[13] S. M. Kay, *Modern Spectral Estimation.* Englewood Cliffs, NJ: Prentice Hall, 1988, ch. 4.

[14] A. McArdle and V. L. Newhouse, "Doppler bandwidth dependence on beam to flow angle," *J. Acoust. Soc. Amer.*, vol. 99, no. 3, pp. 1767–1778, 1996.

[15] K.-W.W. Yeung, "Angle-insensitive flow measurement using Doppler bandwidth," *IEEE Trans. Ultrason., Ferroelect., Freq. Contr.*, vol. 45, no. 3, pp. 574–580, 1998.

[16] A. T. Kerr and J. W. Hunt, "A method for computer simulation of ultrasound Doppler color flow images-I. Theory and numerical method," *Ultrason. Med. Biol.*, vol. 18, no. 10, pp. 861–872, 1992.

[17] ——, "A method for computer simulation of ultrasound Doppler color flow images-II. Simulation results," *Ultrason. Med. Biol.*, vol. 18, no. 10, pp. 873–879, 1992.

[18] M. O'Donnell and W. E. Engeler, "Correlation-based aberration correction in the presence of inoperable elements," *IEEE Trans. Ultrason., Ferroelect., Freq. Contr.*, vol. 39, no. 6, pp. 700–707, 1992.

[19] P.-C. Li and M. O'Donnell, "Phase aberration correction on two-dimensional conformal arrays," *IEEE Trans. Ultrason., Ferroelect., Freq. Contr.*, vol. 42, no. 1, pp. 73–82, 1995.

[20] G. Guidi and S. Falteri, "Phase measurement of acoustic fields based on a moving target," *IEEE Trans. Ultrason., Ferroelect., Freq. Contr.*, vol. 46, no. 3, pp. 679–689, 1999.

[21] J.-Y. Lu and J. F. Greenleaf, "Ultrasonic nondiffracting transducer for medical imaging," *IEEE Trans. Ultrason., Ferroelect., Freq. Contr.*, vol. 37, no. 5, pp. 438–447, 1990.

[22] S. Freeman, P.-C. Li, and M. O'Donnell, "Retrospective dynamic transmit focusing," *Ultrason. Imag.*, vol. 17, no. 3, pp. 173–196, 1995.

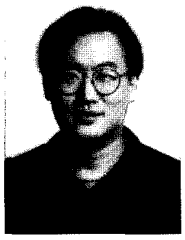

Pai-Chi Li (S'93–M'95) received the B.S. degree in electrical engineering from National Taiwan University, Taipei, Taiwan, R.O.C., in 1987, and the M.S. and Ph.D. degrees from the University of Michigan, Ann Arbor, in 1990 and 1994, respectively, both in electrical engineering: systems.

He was Research Assistant with the Department of Electrical Engineering and Computer Science from 1990 to 1994. He joined Acuson Corporation, Mountain View, CA, as a member of the Technical Staff in June 1994. His work in Acuson was primary in the areas of medical ultrasonic imaging system design for both cardiology and general imaging applications. In August 1997, he went back to the Department of Electrical Engineering at National Taiwan University as Assistant Professor. He then became Associate Professor in August 1998. His current research interests include biomedical ultrasonic imaging and signal processing.

Dr. Li is a member of IEEE, and he was the recipient of the Distinguished Achievement Award in Electrical Engineering: Systems for his outstanding academic achievement at the University of Michigan.

Chong-Jing Cheng was born in Taiwan, R.O.C., on October 6, 1975. He received the B.S. degree in electrical engineering from National Taiwan University in 1998. He is currently a graduate student in the Department of Electrical Engineering at National Taiwan University. His current research interest is ultrasonic flow velocity estimation.

Che-Chou Shen was born in 1976 in Taiwan, R.O.C. He received the B.S. degree from the Department of Electrical Engineering at National Taiwan University in 1998. He is now a graduate student working on ultrasonic harmonic imaging under the instruction of Professor P.-C. Li.